Ultrahigh-permeance PIM-1 based thin film nanocomposite membranes on PAN supports for CO_2 separation

HIGHLIGHTS

High loadings of filler can be incorporated into a polymer film on a porous support

Carbonization enhances the ultramicroporosity of a hypercrosslinked polymer filler

In a thin film, the most significant effects of physical aging occur within 90 days

Aged membranes show high permeance to carbon dioxide

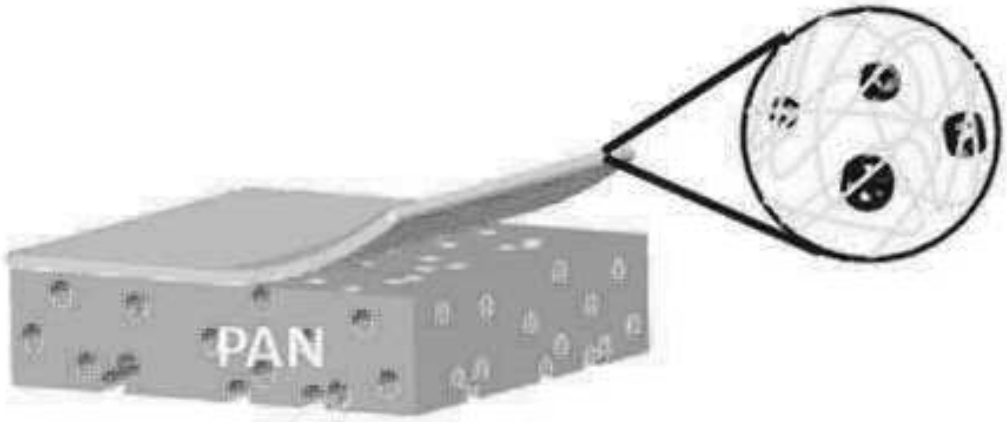

TFN membrane

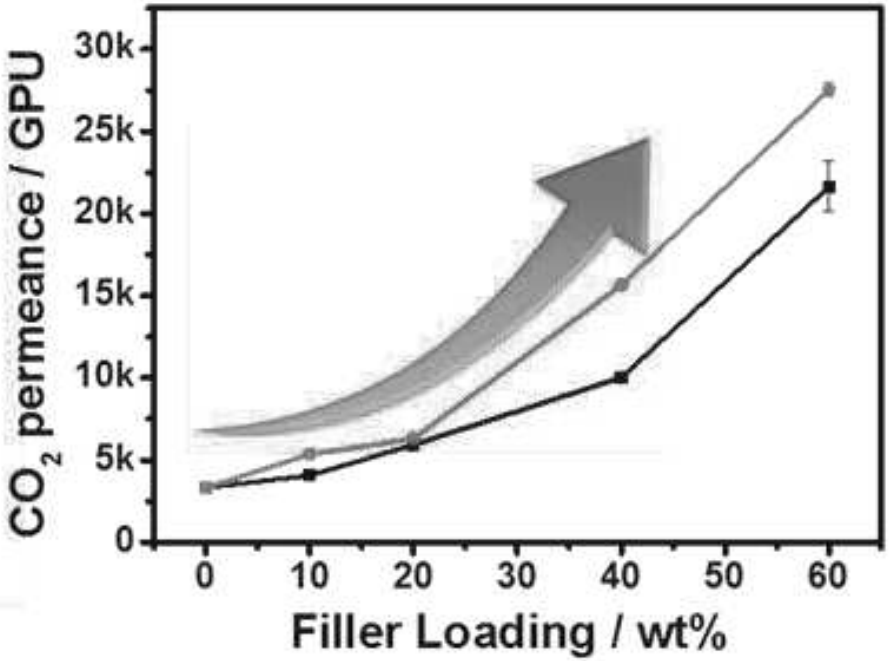

Ultrahigh-permeance PIM-1 based thin film nanocomposite membranes on PAN supports for CO_2 separation

Rupesh S. Bhavsar,[a1] Tamoghna Mitra,[b1] Dave J. Adams,[c*] Andrew I. Cooper,[b*] Peter M. Budd[a*]

[a]School of Chemistry, University of Manchester, Manchester M13 9PL, UK
[b]Department of Chemistry, University of Liverpool, Crown Street, Liverpool, Merseyside L69 7ZD, UK
[c]School of Chemistry, College of Science and Engineering, University of Glasgow, Glasgow, G12 8QQ, UK
[1]These authors contributed equally to this work
[*]Corresponding author
E-mail addresses: Peter.Budd@manchester.ac.uk (Peter.M. Budd), aicooper@liverpool.ac.uk (Andrew I. Cooper), dave.adams@glasgow.ac.uk (Dave J. Adams)

Abstract

High permeance membranes were produced by addition of highly permeable nanoparticulate fillers (hypercrosslinked polystyrene, HCP, and its carbonized form, C-HCP) to a high free volume polymer (polymer of intrinsic microporosity PIM-1) in a thin film (typically 2 μm) on a porous polyacrylonitrile support. Self-standing mixed matrix membranes (MMMs) of thicknesses in the range 40–90 μm were also prepared with the same polymer and fillers. While robust MMMs could only be formed for moderate filler loadings, thin film nanocomposite (TFN) membranes could be produced from dispersions with filler loadings up to 60 wt%. On increasing the filler loading, CO_2 permeance increased in line with the predictions of the Maxwell model for a highly permeable filler. Physical ageing led to some loss of permeance coupled with an increase in CO_2/N_2 selectivity. However, for TFN membranes the greatest effects of ageing were seen within 90 days. After ageing, TFN membranes showed high permeance with reasonable selectivity; for example, with 60 wt% C-HCP, CO_2 permeance > 9,300 GPU, CO_2/N_2 selectivity ~ 11.

Keywords

Carbon capture, hypercrosslinked polymer, polymer of intrinsic microporosity, thin film nanocomposite, mixed matrix membrane

1. Introduction

Capture of CO_2 from the exhaust of a combustion process can help to mitigate climate change [1, 2]. Captured CO_2 can be stored to reduce carbon footprint or serve as an alternative source of carbon for the synthesis of diverse chemicals and fuels (methanol, carboxylic acids, carbonates, polycarbonates, etc.) [3-5]. In recent years, membrane-based processes have emerged as attractive candidates for energy-efficient separations [6-10]. The productivity of a membrane can be expressed in terms of (i) flux, the amount of permeate passing through unit membrane area in unit time, (ii) permeance, the flux normalized for the pressure gradient, or (iii) permeability, the permeance normalized for the membrane thickness. Permeability may be regarded as a property of the membrane material. In general, high selectivity can only be achieved by compromising on permeability and vice versa [11], as demonstrated elegantly by Robeson [12]. However, Merkel et. al. [13] have shown that, under practical conditions for post-combustion carbon capture, higher permeance dominates the economics of the separation process. High selectivity and low permeance necessitates a very large membrane area, which makes it a cost-ineffective process.

Permeance can easily be increased by selecting very thin membranes. However, very thin films are not sufficiently robust for practical use without a highly porous support, which may be of the same material (integrally skinned asymmetric membrane) or of a different material (thin film composite, TFC, membrane). Hägg et al. reported highly selective polyvinyl amine (PVAm) based TFC membranes (selectivity, $\alpha(CO_2/N_2)$ = 50-500) [14-16]. MTR Inc. and Qiao *et. al.* independently reported membranes with moderate selectivity (α ~ 20-50) but with much higher permeance (up to ~ 4000 GPU) [13, 17, 18]. There is a drive to develop even higher permeance membranes that maintain their performance over time.

High-free-volume glassy polymers, such as polymers of intrinsic microporosity (PIMs) or poly[1-(trimethylsilyl)-1-propyne] (PTMSP), are highly permeable to gases such as CO_2 and demonstrate reasonable gas selectivity, making them attractive materials for gas separation membranes [19-22]. A body of work has demonstrated that the addition of fillers into these materials, to form mixed-matrix membranes (MMMs), can increase permeability many fold, as well as reducing the effects of physical ageing [11, 23-26]. However, most research into MMMs has been conducted on relatively thick, self-standing membranes (40–100 μm), which show poor flux due to their thickness. Furthermore, many studies of MMMs have used fillers composed of relatively large particles (>1 μm), which could bridge the entire thickness

of a very thin film. We have previously reported the performance of MMMs of hyper-crosslinked polystyrene (HCP) nanoparticles (diameter *ca*. 55 nm) in the polymer of intrinsic microporosity PIM-1 [11]. Here, we extend that work to thin film nanocomposite (TFN) membranes with a thin coating of mixed-matrix material on a porous polyacrylonitrile (PAN) support, utilizing both HCP nanoparticles and carbonized HCP (C-HCP) nanoparticles as fillers (Figure 1).

2. Experimental

2.1. Materials

Dimethylacetamide (DMAc), toluene, methanol, potassium hydroxide, chloroform, vinylbenzyl chloride, p-divinylbenzene, sodium dodecyl sulphate, potassium persulphate, diethyl ether, 1,2-dichloroethane (DCE) and ferric chloride ($FeCl_3$) were purchased from Sigma-Aldrich and used as received. Tetrafluoroterephthalonitrile (TFTN, 98%, Aldrich) was purified by sublimation; it was heated to around 150 ºC and the pure product collected without vacuum. 5,5',6,6',-Tetrahydroxy-3,3,3',3'-tetramethyl-1,1'-spirobisindane (THSBI, 98%, Alfa Aesar) was dissolved in methanol and re-precipitated from dichloromethane before use. Anhydrous potassium carbonate (K_2CO_3, 99.0%, Fisher) was dried in an oven at 110 ºC overnight before use. Porous polyacrylonitrile (PAN) membrane (Sepro PA350 ultrafiltration membrane) was kindly provided by Prof. Ingo Pinnau, King Abdullah University of Science and Technology, Saudi Arabia.

2.2. Synthesis of PIM-1, HCP nanoparticles and carbonized HCP nanoparticles

PIM-1 and hypercrosslinked polystyrene (HCP) nanoparticles were synthesized as reported previously and details are summarized in the supporting information [11, 27]. Carbonization of HCP nanoparticles (carbonized product referred to as C-HCP) followed a previously reported procedure [28]: 0.5 g of HCP and 2 g of potassium hydroxide were mixed using a mortar and pestle. The mixture was then transferred to an alumina boat and the boat was placed in an oven. The temperature of the oven was raised to 800 °C at a rate of 5 °C min^{-1}. The oven temperature was then maintained at 800 °C for 2 h under a gentle N_2 flow. The oven was then allowed to cool to ambient temp. The dark mass was washed with 1 L water, followed by 200 mL methanol. It was then dried at 100 °C under vacuum.

2.3. Gas sorption analysis

Nitrogen adsorption and desorption isotherms at 77.3 K and 298 K, and CO_2 adsorption and desorption isotherms at 298 K, were measured using a Micromeritics ASAP 2020 volumetric adsorption analyzer. Samples were degassed offline at 60 °C for 12 h under vacuum (10^{-5} bar) before analysis, followed by degassing on the analysis port under vacuum.

2.4. Membrane preparation

TFN membranes of PIM-1/HCP and PIM-1/C-HCP on PAN supports were prepared by dip coating with 3% w/v total solids in chloroform ($CHCl_3$). Coating solutions were prepared with four different proportions of filler to total solids (10, 20, 40 and 60 wt%). For example, for 10 wt% filler, a suspension of filler (0.03 g) in 5 mL $CHCl_3$ was stirred for 12 h at ambient temperature, followed by sonication for 30 min in a Bandelin Sonorex ultrasonic bath at ambient temperature. A solution of PIM-1 (0.27 g in 5 mL $CHCl_3$) was added to the suspension and stirred for 20 h. The resulting solution was sonicated for 20 min in an ultrasonic bath at ambient temperature before being used for dip coating. A PAN support was dried under vacuum at ambient temperature for 1 h, then a piece (63×45 mm) was fixed on a glass slide and the edge sealed with aluminium tape, to ensure only the PAN-coated side of the support came into contact with coating solution. The glass slide was then dipped vertically into a tray filled with coating solution. It was kept immersed for 2 s at ambient temperature, and then removed slowly. The TFN membranes were rested on a horizontal surface for 24 h and then kept in a vacuum desiccator for 2 h, in order to remove the residual solvent. It is known that membrane performance depends on drying parameters, as demonstrated previously [29-31]. For better comparison with previous work, all the membranes were dried at room temperature. Self-standing MMM membranes were prepared by the solution casting method as reported previously [11] and described in the supporting information.

2.5. Membrane characterization

The average pore size of the PAN membrane was measured by a Porolux™ 1000 Porometer. The membrane morphology was studied by scanning electron microscopy (SEM) using a Hitachi S-4800 Field-Emission Scanning Electron Microscope with Energy Dispersive X-Ray (EDX) detector and cold cathode electron source. The membrane cross section was

prepared via freeze fracturing using liquid nitrogen. The sample was then coated with gold by sputtering using an Emitech coater.

2.6. Gas permeation measurements

The permeability measurements using pure gases (CO_2 and N_2) were carried out by the standard variable volume method [32] (see supporting information) at an upstream gas pressure of 2 atm and at ambient temperature (~ 298 K), while maintaining the permeate side at the atmospheric pressure. Membrane samples (2.5 cm in diameter), after removing from the vacuum desiccator, were immediately mounted in the permeation cell. For ageing analysis, all the membranes were stored in a sealed petri dish at room temperature. The CO_2 and N_2 pure gas permeability after ageing was carried out at 2 atm upstream pressure and at ambient temperature. The gas permeance was calculated using eq. 1:

$$K = \frac{Q}{tA(p_1 - p_2)} . 10^{-6} \quad (1)$$

where K is the permeance in gas permeation units (1 GPU = 10^{-6} cm^3[STP] cm^{-2} s^{-1} $cmHg^{-1}$ = 3.348×10^{-10} mol m^{-2} s^{-1} Pa^{-1}), Q is the volume of permeated gas (cm^3, adjusted to STP [0°C, 1 atm]), t is the permeation time (s), A is the membrane area (cm^2), and p_1 and p_2 are the feed and permeate side pressures (cmHg), respectively. Gas permeability was calculated using eq 2:

$$P = \frac{Q\, l}{tA(p_1 - p_2)} .10^{-10} \quad (2)$$

where l is the membrane thickness (cm) and P is the permeability coefficient expressed in barrer (1 barrer = 10^{-10} cm^3[STP] cm cm^{-2} s^{-1} $cmHg^{-1}$ = 3.348×10^{-16} mol m m^{-2} s^{-1} Pa^{-1}).

3. Results and discussion

3.1. Fillers for TFN membranes

We investigated two highly porous nanoparticulate fillers, a hypercrosslinked polystyrene (HCP) and its carbonised version (C-HCP). These fillers are easily prepared using inexpensive starting materials [11, 28]. Figure 2(a) compares the N_2 adsorption/desorption isotherms at 77 K for PIM-1, HCP and C-HCP. The polymer and fillers exhibit high uptake at

low relative pressure, characteristic of a microporous material as defined by IUPAC (pore size <20 Å) [33]. N_2 uptakes increase in the sequence PIM-1 < HCP < C-HCP, reflected in Brunauer–Emmett–Teller (BET) surface areas of 790, 1750 and 2700 $m^2 g^{-1}$ for PIM-1, HCP and C-HCP, respectively. Micropore volumes of the fillers were estimated from the N_2 adsorption isotherms. As generally observed for microporous polymers, the adsorption isotherms exhibit a positive slope in the relative pressure range 0.4-0.8, which may be attributed to swelling by the penetrant. We therefore extrapolated these data linearly to zero relative pressure to obtain an estimate of the uptake of N_2 that can be attributed to the porosity of the filler. Hence, the bulk densities were evaluated as 0.65 g cm^{-3} for HCP and 0.57 g cm^{-3} for C-HCP, taking the skeletal densities to be those for polystyrene (1.05 g cm^{-3} [34]) and graphite (2.26 g cm^{-3} [35]), respectively. For HCP, this is within the range of densities previously reported for similar materials (0.35 [36], 0.78, 0.42 [37]). Analysis of the low pressure region of the adsorption isotherms by the Horvath-Kawazoe method [38] (Figure 2(b)) indicates a higher level of ultramicroporosity (pore size < 7 Å) in C-HCP than in HCP. The combination of small pore size and high porosity makes these fillers interesting candidates for nanocomposite membranes.

Figure 3 shows CO_2 and N_2 adsorption/desorption isotherms at 298 K. After carbonization, the CO_2 uptake is more than double that of HCP, reflecting the higher level of ultramicroporosity in C-HCP [39]. The higher CO_2 adsorption is helpful to improve the CO_2 permeability, as permeability depends on sorption and diffusivity [40]. The HCP particles retain their nanoparticulate morphology after carbonization (see supporting information). The thermal stabilities were investigated by thermogravimetric analysis (see supporting information). Thermal stability was improved by carbonization, the C-HCP showing only a small weight loss up to 800 °C under N_2.

3.2. TFN membranes

TFN membranes were prepared by dip-coating a PAN support (thickness 150 μm; pore size ~ 31 nm with a narrow distribution, see supporting information) with a dispersion of the filler in a solution of PIM-1 in chloroform. For comparison, self-standing MMMs with thicknesses in the range 40–90 μm were also prepared, by casting on a glass mould. TFN membranes could be prepared from coating solutions with ~ 60 wt% filler loading, while with self-

standing MMMs the filler could be loaded only up to 17 wt%. After ethanol treatment, at higher C-HCP loading in a self-standing membrane, a very brittle and curly membrane was formed (see supporting information). This membrane was difficult to handle and hence could not be analysed. The filler becomes the dominant phase in terms of volume fraction at loadings above 38 wt% for HCP and 35 wt% for C-HCP, taking the bulk densities for HCP, C-HCP and PIM-1 to be 0.65, 0.57 (see above) and 1.056 [41], respectively. Images from scanning electron microscopy (SEM) of TFN membranes at low and high loading are included in Figure 1. A well-defined thin (~ 2 μm) film with a homogeneous distribution of filler was achieved at low filler loadings, but at high loadings an irregular layer of varying thickness was formed. Apparent thicknesses of the selective layer from SEM images of TFN membranes are given in the supporting information.

3.2. Gas permeation analysis

3.3.1. Effect of filler loading on permeance and selectivity

Figure 4a shows how CO_2 permeance varies with filler loading for unaged PIM-1/HCP and PIM-1/C-HCP TFN membranes (see supporting information for tabulated data). Both fillers give a marked increase in permeance with increase in filler loading, showing increases compared to pristine PIM-1 of up to ~ 550% with HCP and ~ 725% with C-HCP, in accordance with the high porosity and high internal surface area of HCP, and even higher values for C-HCP, as seen in Figure 2. For comparison, Figure 4c shows the variation of CO_2 permeability with filler loading for self-standing PIM-1/C-HCP MMMs, both "as cast" and after ethanol-treatment. Equivalent data for PIM-1/HCP MMMs have been reported previously [11]. It should be noted that self-standing, "as cast" MMMs with C-HCP show a higher increase in CO_2 permeability (~ 475% at 17 wt.% filler) than previously reported MMMs with HCP (~ 277%) [11], demonstrating the benefit of carbonized filler for improving gas permeability.

The effect of filler loading on CO_2/N_2 selectivity is shown in Figure 4b for PIM-1/HCP and PIM-1/C-HCP TFN membranes, and in Figure 4d for self-standing, "as cast" PIM-1/C-HCP MMMs. For TFN membranes, the dramatic increase in permeance on addition of filler is accompanied by a significant drop in selectivity. This could be due to the presence of microvoids in the selective layer, arising from poor packing of the filler or poor adhesion with the polymer matrix. Microvoids may provide high permeability pathways for both gases. Selectivity improves on ageing the membrane, as discussed later.

A number of models may be employed to describe the permeation of gases through a composite comprising a dispersed filler in a continuous matrix. One of the simplest is the Maxwell model, which was originally developed for electrical conductivity [42], but can equally be applied to gas permeation [43]. The effective permeability of a mixed matrix membrane, P_{MMM}, depends on the volume fraction of the dispersed phase, Φ_d, and on the permeabilities of the dispersed and continuous phases, P_d and P_c, respectively, according to:

$$P_{MMM} = P_c\left[\frac{P_d + 2P_c - 2\Phi_d(P_c - P_d)}{P_d + 2P_c + \Phi_d(P_c - P_d)}\right] \quad (3)$$

Two limiting cases may be considered. At one extreme, if the dispersed phase is completely impermeable ($P_d = 0$), the Maxwell equation simplifies to

$$P_{MMM} = P_c\left[\frac{1 - \Phi_d}{1 + 0.5\Phi_d}\right] \quad (4)$$

At the other extreme, if the dispersed phase has extremely high permeability ($P_d \to \infty$), the Maxwell equation simplifies to:

$$P_{MMM} = P_c\left[\frac{1 + 2\Phi_d}{1 - \Phi_d}\right] \quad (5)$$

Figure 5 compares experimental data for CO_2 and N_2 permeance of the TFN membranes with the limiting cases of the Maxwell model, assuming the effective thickness of the active layer does not vary significantly with filler loading. It can be seen that the experimental data fall close to the upper limit, demonstrating that the filler provides high permeability pathways for gas transport. The Maxwell model gives a good description of the behaviour even at high loadings where it would not normally be expected to apply. Figure 6 shows similar plots for CO_2 and N_2 permeability of self-standing MMMs, demonstrating that the performance is close to the Maxwell upper limit over the range of filler loadings achievable.

3.3.2. Effect of ageing on permeance and selectivity

One of the most significant issues for membrane gas separations with PIMs and other high free volume glassy polymers is that of physical ageing; that is, changes in properties that occur over time, arising from the non-equilibrium nature of the glassy state. For a thick, self-standing membrane, measurable reductions in permeability may occur over very long

timescales (> 4 years) [44]. These effects can be at least partially reversed by an alcohol treatment (immersion in methanol or ethanol overnight, then allowing the alcohol to evaporate), and self-standing membranes are commonly studied after an alcohol treatment to reset the ageing clock. However, such treatments often cannot be applied to thin film composite membranes, because they may lead to delamination of the selective layer. Physical ageing, while leading to a loss of permeability, is often accompanied by an increase in selectivity, and in favourable cases aged membranes may have positive advantages for gas separation, providing that the initial membrane permeance is high enough. The rate of physical ageing depends on film thickness, being much more rapid in very thin films than in thick films [45-48]. Harms *et al*. [49] used depth-resolved positron annihilation lifetime spectroscopy to investigate free volume changes over time in PIM-1 films of various thicknesses. They concluded that in films with thickness < 1 μm, ageing is nearly complete after 3 months, whereas for films with thickness > 1 μm, ageing continues even after several months. This suggests that stable membranes suitable for commercial use may be achieved after relatively short ageing times for thin film composite membranes with very thin active layers: indeed, the long-term stability of the support may be of greater concern than changes to the selective layer. Here we sought to confirm the timescale over which ageing effects are significant for TFN membranes, and to investigate the performance that can be achieved in aged membranes.

Figure 7 shows the changes in CO_2 permeance and CO_2/N_2 selectivity over time for PIM-1/C-HCP and PIM-1/HCP TFN membranes. It can be seen that during the first week of ageing there is a substantial loss of permeance accompanied by an increase in selectivity, with more moderate changes occurring over the following few weeks. In contrast, it can be seen in Figure 8 that after six months the transport properties of self-standing MMMs continue to show significant changes with time. This is consistent with the conclusions of Harms *et al.* [49].

Bernardo *et al*. [44] have shown that ageing in PIM-1 mainly affects the diffusion coefficient for permanent gases, and that molecules with larger kinetic diameter are affected more by physical ageing than smaller molecules. The kinetic diameters of N_2 and CO_2 are 3.64 Å and 3.3 Å, respectively [50], so the diffusion of N_2 is more restricted and selectivity improves on initial ageing. This may be reinforced by a favourable sorption term for CO_2. For aged PIM-1/C-HCP TFN membranes, reasonable selectivity can be achieved in combination with very

high permeance, *e.g.,* a TFN membrane with 60 wt% C-HCP after 90 days has CO_2 permeance >9,300 GPU with a CO_2/N_2 selectivity of ~ 11.

A Robeson plot [12] of selectivity against permeability provides a useful basis for comparing the performance of different membrane materials and assessing whether ageing has a positive effect (*e.g.*, leading to performance further above the upper bound). Figure 9 compares data for TFN membranes from this work with data for self-standing MMMs. For TFN membranes, the gas permeances were converted to permeabilities by multiplying by the average thickness of the selective layer as measured by SEM. It is noteworthy that PIM-1/C-HCP TFN membranes at high loadings exceed the 2008 upper bound while exhibiting very high apparent permeabilities, and exhibit comparable performance to recently reported highly permeable PIMs (PIM-TMN-Trip and PIM-TMN-SBI [51], showing considerable promise for CO_2 separation.

Figure 10 compares the CO_2 permeation properties of two TFN membranes from this work with data from the literature for other thin film composites. It is clear that PIM-1/C-HCP TFN membranes offer exceptional permeance. Although the selectivity of the best performing membrane reported here (PIM-1/C-HCP, 60 wt%, CO_2/N_2 selectivity ~ 11, $K(CO_2)$ > 9,300 GPU) is lower than that of the POLARIS-3 membrane (CO_2/N_2 selectivity ~ 22, $K(CO_2)$ ~ 4000 GPU) [18], it shows significantly higher permeance. There is scope to improve the selectivity of PIM-based TFN membranes, as indicated by the higher selectivities of aged self-standing MMMs, as well as to further enhance permeance by forming even thinner selective layers. A key difference between the TFN membranes and the self-standing MMMs reported here is that solvent evaporation is extremely rapid when $CHCl_3$ is used as a solvent for dip-coating to form a TFN membrane. By contrast, very slow evaporation conditions are employed when solution casting to form self-standing MMMs. Future work will explore ways of controlling the formation of the selective layer in a TFN membrane. It is also important to note that flue gas for coal-fired power plants contains 3-4 % water vapour and trace amounts of impurities such as SO_2 [52]. It is known that the presence of water vapour can cause a reduction in the CO_2 separation performance through competitive sorption and water clustering effects, as the water molecules in the membrane occupy free volume that would otherwise be occupied by CO_2 [53]. Thus, the effect of water vapour on CO_2 separation performance of the TFN membrane will need to be explored in the future.

4. Conclusions

Thin film nanocomposite (TFN) membranes, with selective layers of nanoparticulate fillers in the glassy polymer PIM-1, offer exceptional permeance for CO_2 separation. Carbonised hypercrosslinked polystyrene (C-HCP) nanoparticles have higher internal surface area and greater ultramicroporosity than the uncarbonised form (HCP), imparting greater increases in permeance. Very high filler loadings (up to 60 wt%) could be achieved in TFN membranes, but not in self-standing MMMs. The increase in permeance with increasing filler loading was consistent with the predictions of the Maxwell model for a highly permeable filler. For TFN membranes, the most significant effects of physical ageing, which leads to some loss of permeance coupled with an increase in selectivity, are seen within 90 days, whereas self-standing mixed matrix membranes (MMMs) continue to age significantly beyond 200 days. After ageing, TFN membranes show high permeance with reasonable selectivity, (*e.g.*, with 60 wt% C-HCP, $K(CO_2) > 9{,}300$ GPU, CO_2/N_2 selectivity ~ 11). We believe that this represents a useful design strategy for cost-effective and scalable TFN membranes for gas separations.

Acknowledgements

We thank the EPSRC for funding (EP/M001342/1). D. A. thanks the EPSRC for a Fellowship (EP/L021978/1). We thank Prof. Ingo Pinnau, King Abdullah University of Science and Technology, who kindly provided PAN membrane.

Appendix A - Supporting information

Supplementary data associated with this article can be found in the online version. All research data supporting this publication are directly available within this publication and the supporting information, as well as available from the corresponding authors upon reasonable request.

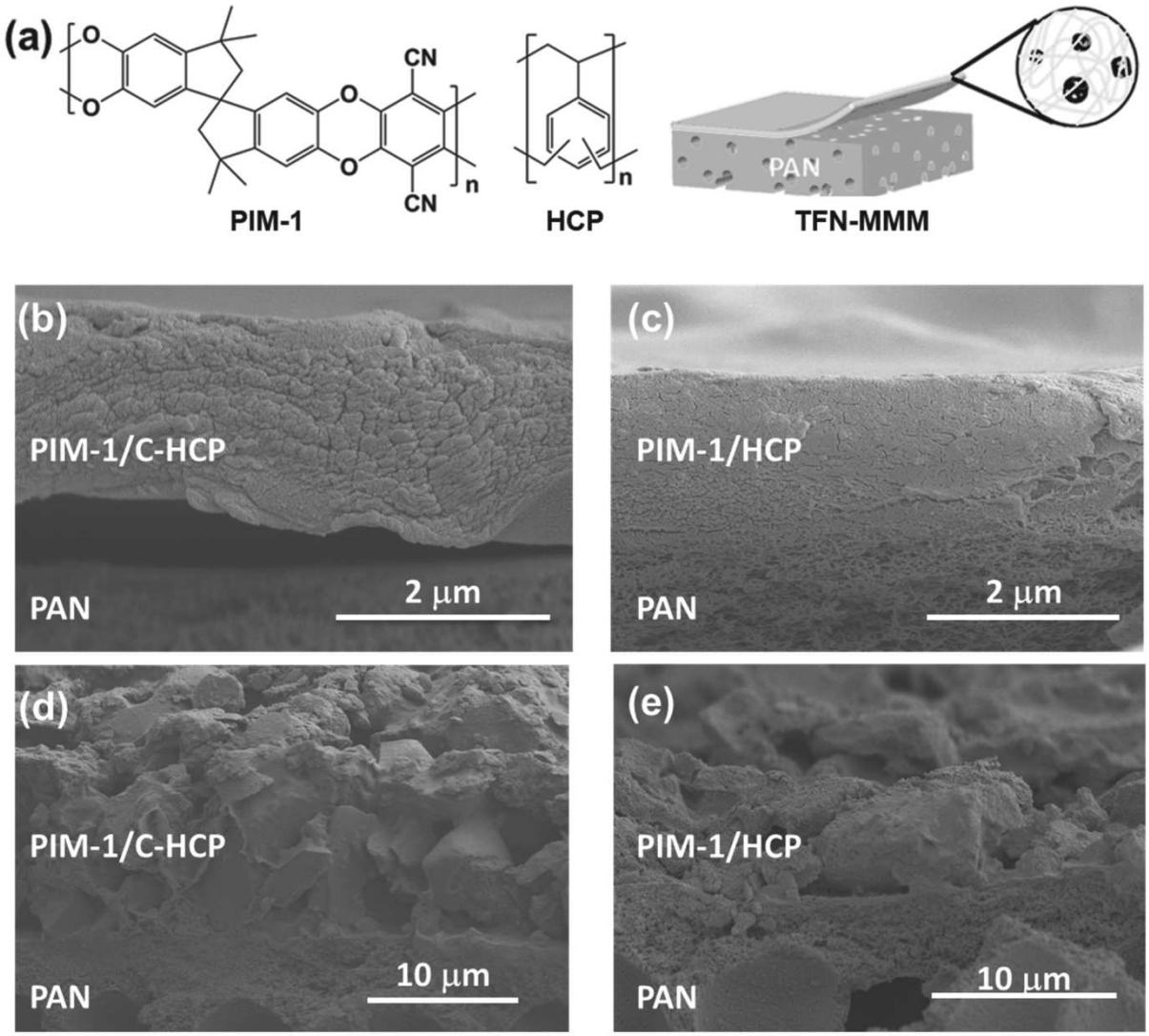

Fig. 1. (a) Molecular structures of PIM-1 and HCP, and schematic illustration of a thin-film nanocomposite membrane, with a selective layer of PIM-1 with nanoparticulate HCP or C-HCP filler, on a highly porous PAN support. SEM images of (b, d) thin film nanocomposite of PIM-1/C-HCP and (c, e) thin film nanocomposite of PIM-1/HCP. The images shown in (b) and (c) represent lower filler concentration (10 wt%), whilst those in (d) and (e) represent higher filler concentration (60 wt%).

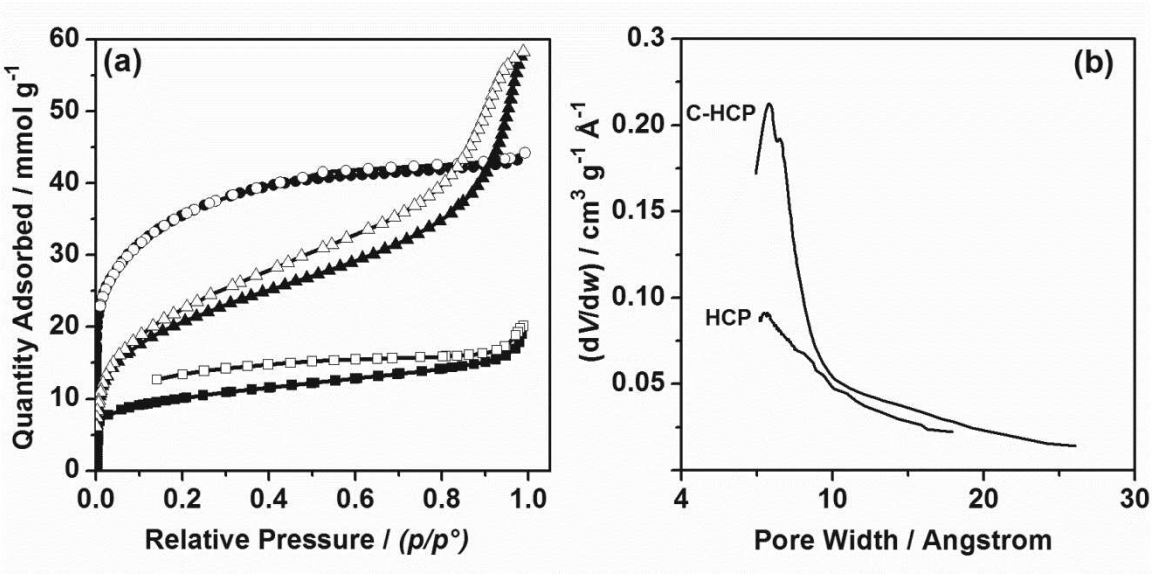

Fig. 2. (a) Nitrogen adsorption (filled symbols) and desorption (open symbols) isotherms at 77 K for PIM-1 (■,□), HCP (▲,△) and C-HCP (●,○). (b) Pore size distributions for HCP and C-HCP determined from N_2 adsorption data by the Horvath-Kawazoe method.

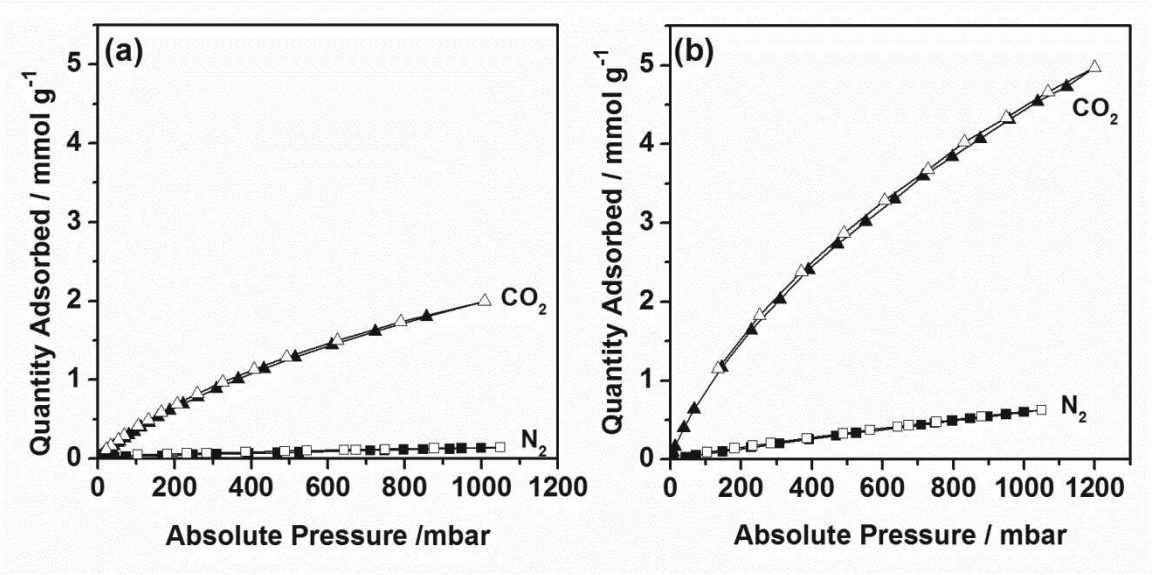

Fig. 3. CO_2 and N_2 adsorption (filled symbols) and desorption (open symbols) isotherms at 298 K for (a) HCP and (b) C-HCP nanoparticles.

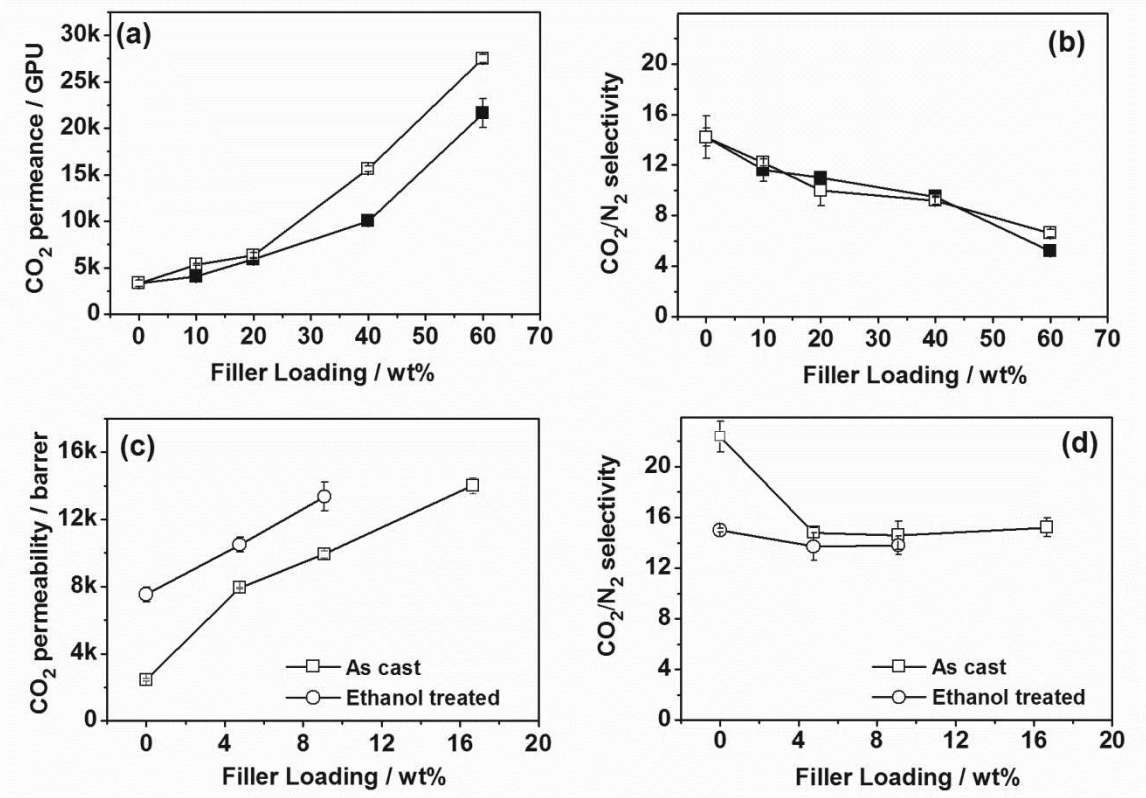

Fig. 4. Dependence of (a) CO_2 permeance and (b) CO_2/N_2 selectivity for TFN membranes (solid symbol represents PIM/HCP TFN membranes and open symbol represents PIM/C-HCP TFN membranes). Dependence of (c) CO_2 permeability and (d) CO_2/N_2 selectivity for self-standing as cast and ethanol treated PIM-1/C-HCP MMMs. All data are shown for non-aged membranes. Error bar represents the standard deviation of 3 samples. The CO_2 permeability and CO_2/N_2 selectivity for PIM-1/HCP MMMs were reported previously [11].

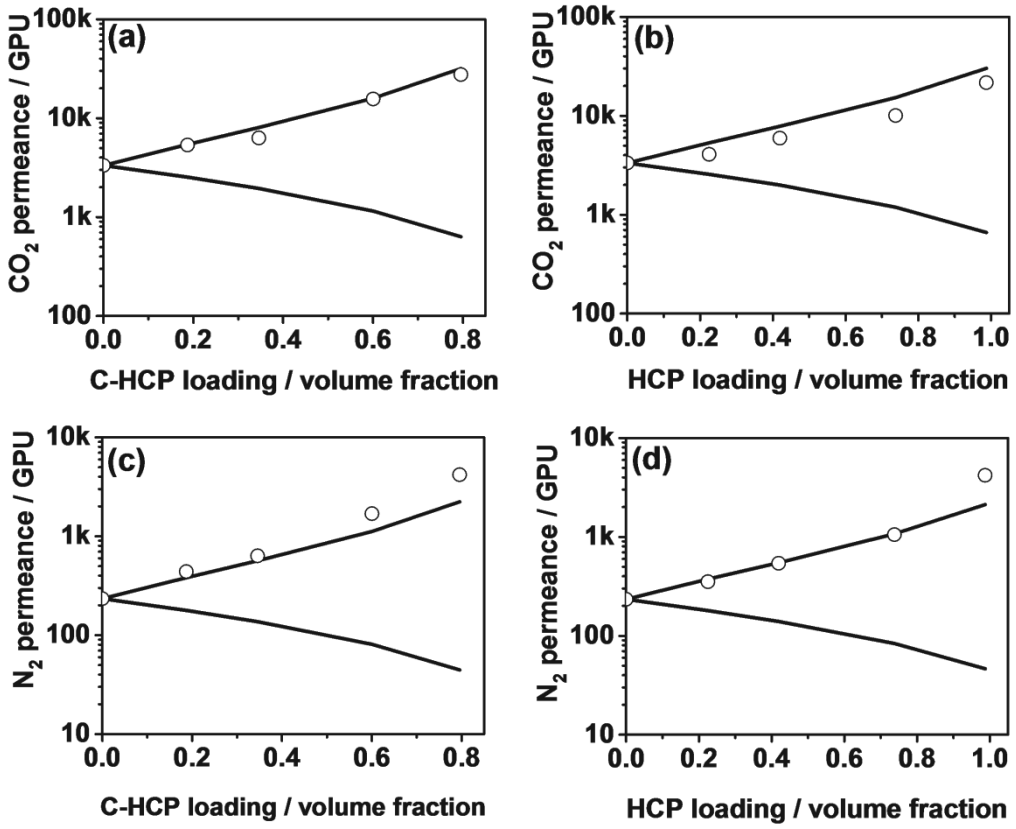

Fig. 5. Dependence of (a, b) CO_2 permeance and (c, d) N_2 permeance on filler loading for (a, c) PIM-1/C-HCP and (b, d) PIM-1/HCP TFN membranes. The open circles represent experimental data and the lines correspond to the predictions of the Maxwell model for the limits of an impermeable filler ($P_d = 0$, lower line) and a very highly permeable filler ($P_d \rightarrow \infty$, upper line).

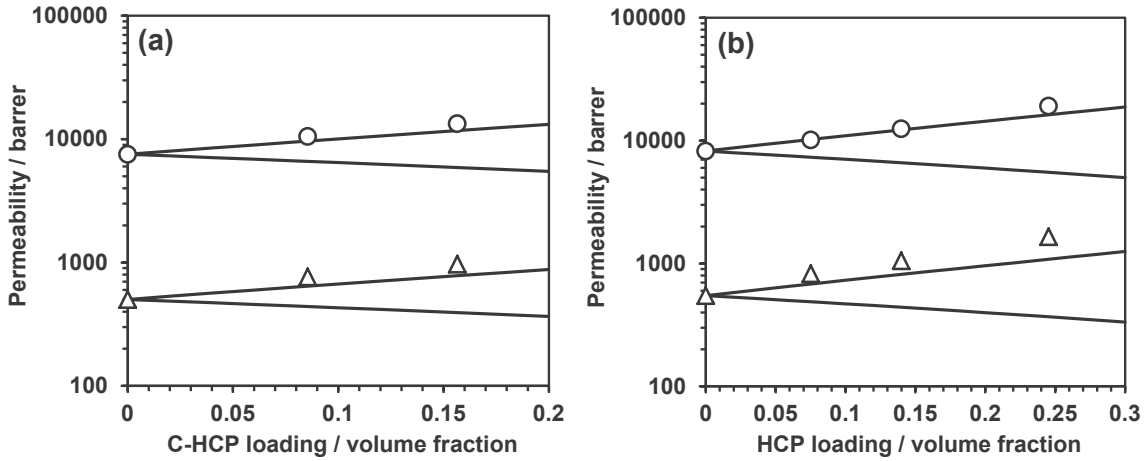

Fig. 6. Dependence of CO_2 permeability (○) and N_2 permeability (△) on filler loading for (a) PIM-1/C-HCP and (b) PIM-1/HCP based self-standing, ethanol-treated MMMs. The solid lines correspond to the predictions of the Maxwell model for the limits of an impermeable filler ($P_d = 0$, lower line of each pair) and a very highly permeable filler ($P_d \rightarrow \infty$, upper line of each pair).

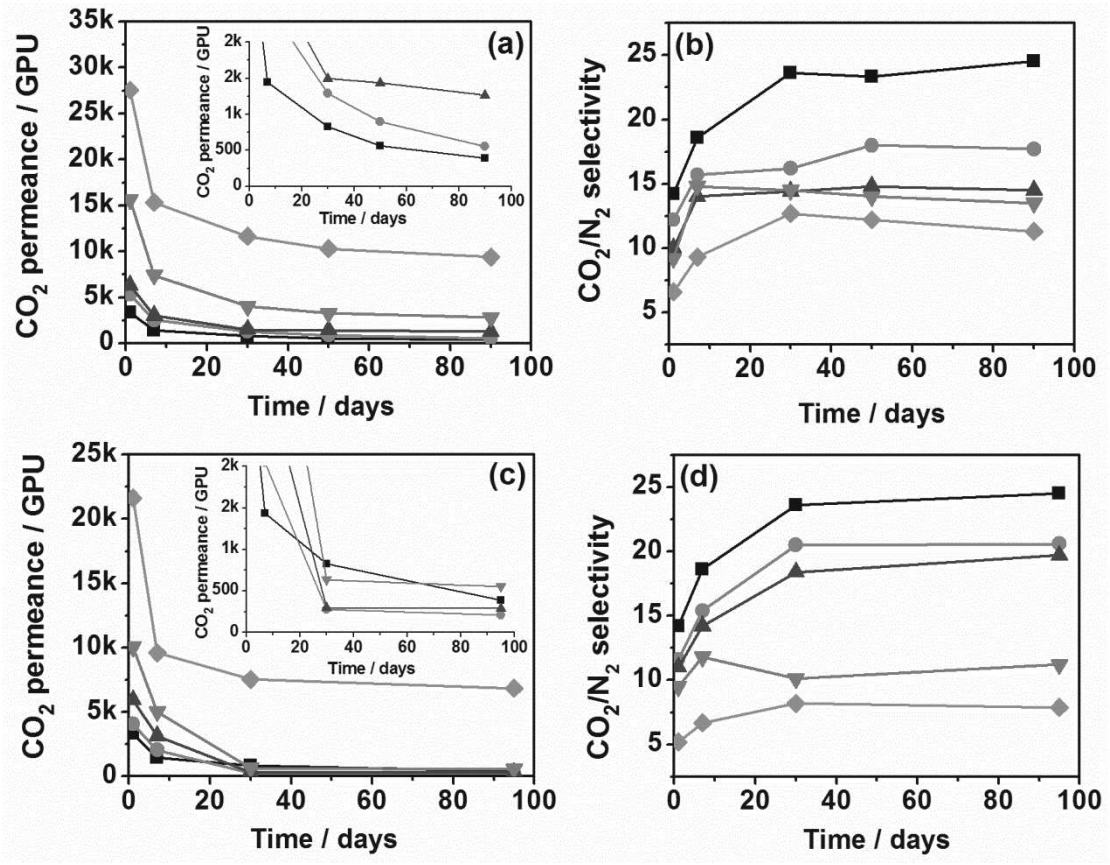

Fig. 7. Changes in (a, c) CO_2 permeance and (b, d) CO_2/N_2 selectivity of TFN membranes over time with (a, b) C-HCP as filler and (c, d) HCP as filler, at filler loadings of 0 wt% (■), 10 wt% (●), 20 wt% (▲), 40 wt% (▼) and 60 wt% (◆).

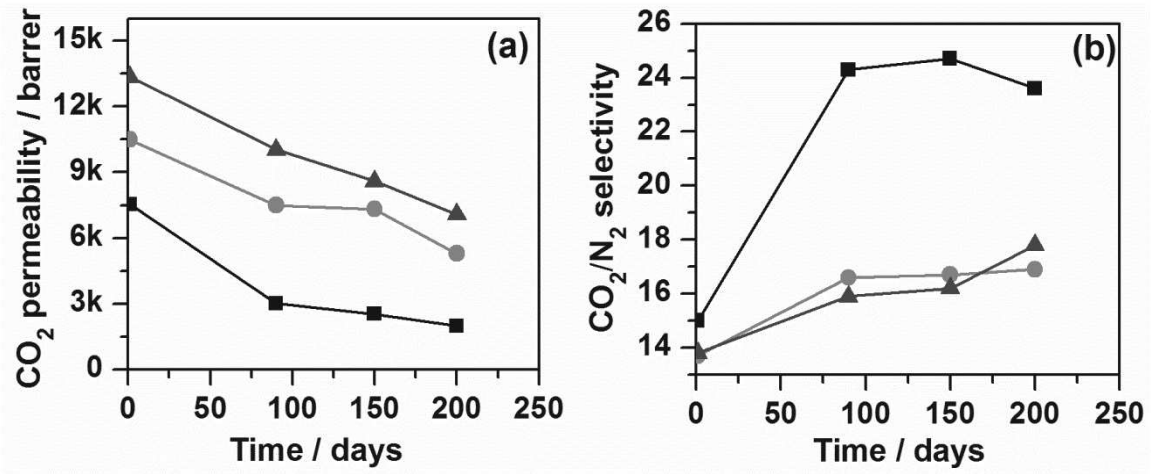

Fig. 8. Changes in (a) CO_2 permeability and (b) CO_2/N_2 selectivity of self-standing ethanol-treated PIM-1/C-HCP MMMs over time, with filler loadings of 0 wt% (■), 4.76 wt% (●) and 9.1 wt% (▲).

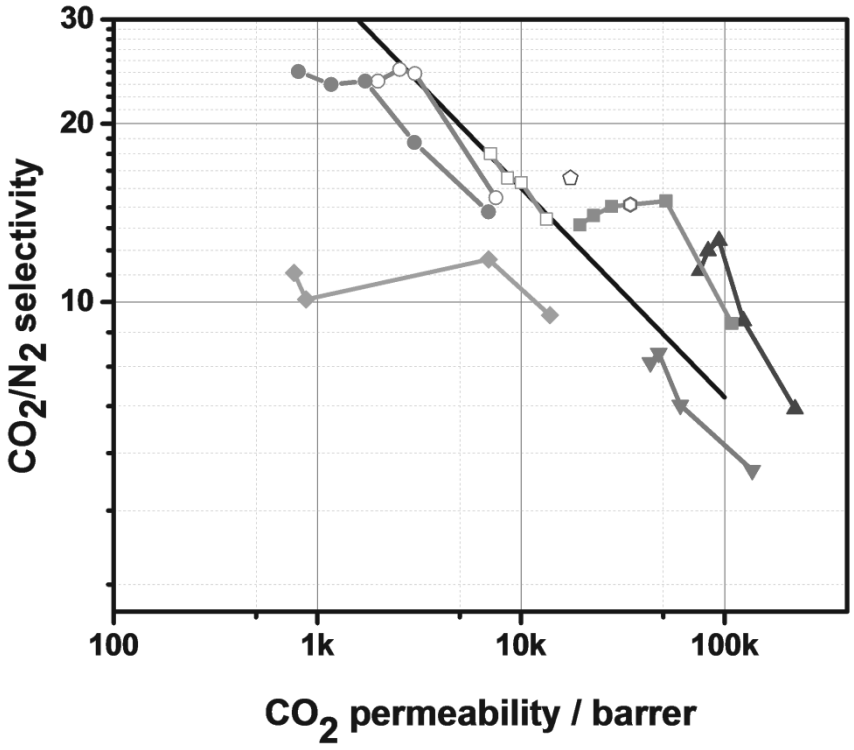

Fig. 9. Robeson plot of ideal CO_2/N_2 selectivity against apparent CO_2 permeability showing Robeson's 2008 upper bound (solid line) and experimental data for TFN membranes of PIM-1(●), PIM-1/C-HCP 40 wt% (■), PIM-1/C-HCP 60 wt% (▲), PIM-1/HCP 40 wt% (◆) and PIM-1/HCP 60 wt % (▼) after various aging times (1→90 days), and for self-standing ethanol treated MMMs of PIM-1(○) and PIM-1/C-HCP 10 wt% (□) after various aging times (1→90 days), and high performing PIMs, PIM-TMN-Trip (⬡) and PIM-TMN-SBI (⬠) [[51]].

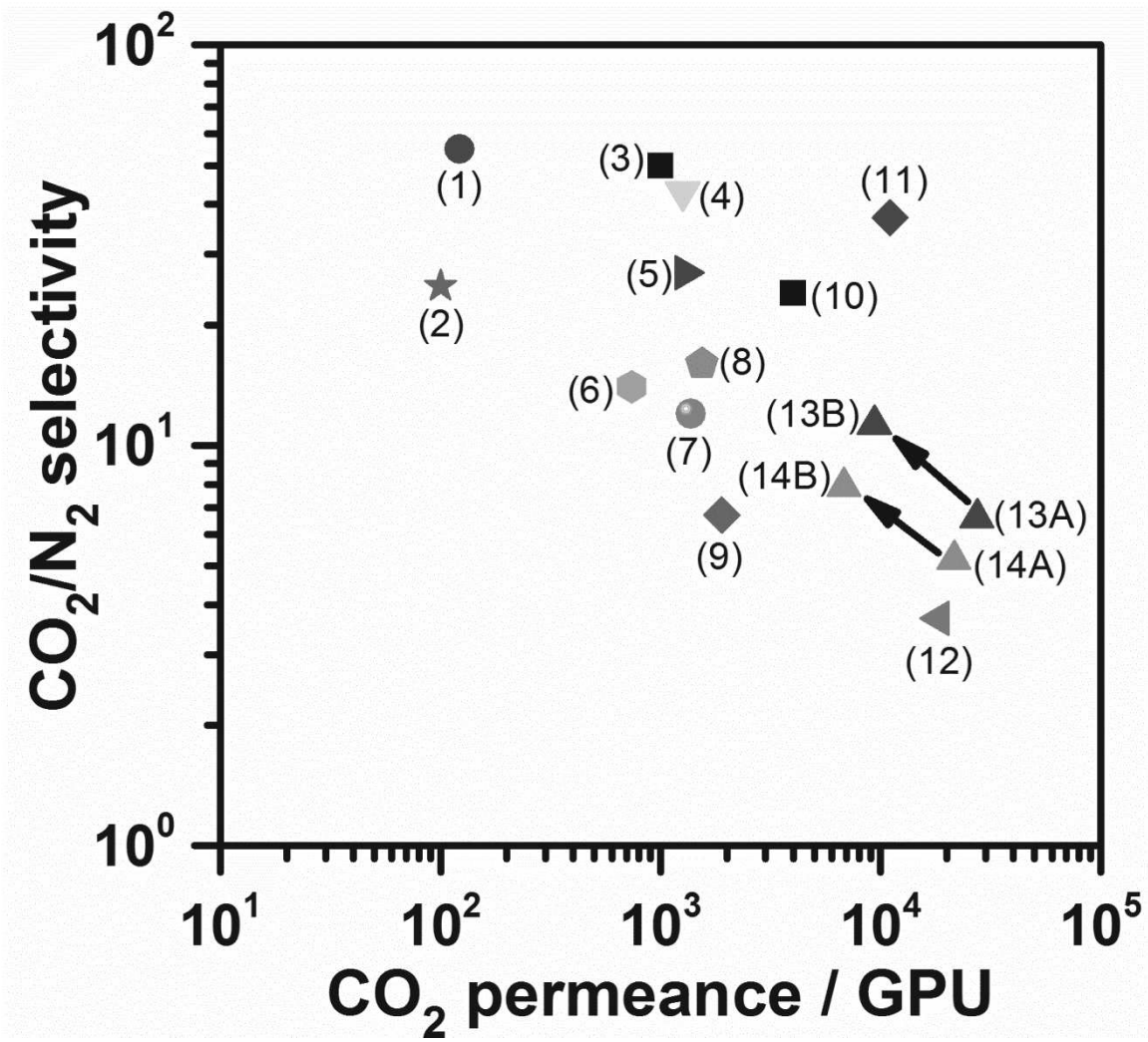

Fig. 10. Summary of the CO_2 permeation properties of selected TFN membranes presented in this work, in comparison with data for other thin film composites. (1) PEBAX1657/PEG [54], (2) commercial natural gas membrane [13], (3) Polaris-1™ [13], (4) PEG based UFC membrane [55], (5) PDA-PEI/SiO_2 [17], (6) PMDA-ODA [56], (7) Pebax®2533/grafted star polymer [57], (8) BPVE-PFCB [58], (9) PTMSP/PAF [59], (10) Polaris-3™ [18], (11) PIM-1/f-MWCNT [60], (12) Cross linked PTMSP [61], (13A-B) PIM-1/C-HCP TFN membrane (60 wt%, A: 1 day, B: 90 days), (14A-B) PIM-1/HCP TFN membrane (60 wt%, A: 1 day, B: 90 days)

References

[1] R. Quadrelli, S. Peterson, The energy–climate challenge: Recent trends in CO_2 emissions from fuel combustion, Energy Policy, 35 (2007) 5938-5952.
[2] K. Sumida, D.L. Rogow, J.A. Mason, T.M. McDonald, E.D. Bloch, Z.R. Herm, T.-H. Bae, J.R. Long, Carbon Dioxide Capture in Metal–Organic Frameworks, Chem. Rev., 112 (2012) 724-781.
[3] Carbon Dioxide Recovery and Utilization, first ed., Springer, The Netherlands, 2003.
[4] J. Artz, T.E. Muller, K. Thenert, J. Kleinekorte, R. Meys, A. Sternberg, A. Bardow, W. Leitner, Sustainable Conversion of Carbon Dioxide: An Integrated Review of Catalysis and Life Cycle Assessment, Chem. Rev., 118 (2018) 434-504.
[5] J. Albo, M. Alvarez-Guerra, P. Castano, A. Irabien, Towards the electrochemical conversion of carbon dioxide into methanol, Green Chem., 17 (2015) 2304-2324.
[6] R.W. Baker, Future Directions of Membrane Gas Separation Technology, Ind. Eng. Chem. Res., 41 (2002) 1393-1411.
[7] M.G. Buonomenna, Membrane processes for a sustainable industrial growth, RSC Adv., 3 (2013) 5694-5740.
[8] J. Dechnik, J. Gascon, C. Doonan, C. Janiak, C.J. Sumby, New directions for mixed-matrix membranes, Angew. Chem. Int. Edn., 56 (2017) 9292-9310.
[9] G. Dong, H. Li, V. Chen, Challenges and opportunities for mixed-matrix membranes for gas separation, J. Mater. Chem. A, 1 (2013) 4610-4630.
[10] W.J. Koros, C. Zhang, Materials for next-generation molecularly selective synthetic membranes, Nat. Mater., 16 (2017) 289-297.
[11] T. Mitra, R.S. Bhavsar, D.J. Adams, P.M. Budd, A.I. Cooper, PIM-1 mixed matrix membranes for gas separations using cost-effective hypercrosslinked nanoparticle fillers, Chem. Commun., 52 (2016) 5581-5584.
[12] L.M. Robeson, The upper bound revisited, J. Membr. Sci., 320 (2008) 390-400.
[13] T.C. Merkel, H. Lin, X. Wei, R. Baker, Power plant post-combustion carbon dioxide capture: An opportunity for membranes, J. Membr. Sci., 359 (2010) 126-139.
[14] L. Deng, T.-J. Kim, M.-B. Hägg, Facilitated transport of CO_2 in novel PVAm/PVA blend membrane, J. Membr. Sci., 340 (2009) 154-163.
[15] T.-J. Kim, B. Li, M.-B. Hägg, Novel fixed-site–carrier polyvinylamine membrane for carbon dioxide capture, J. Polym. Sci. Part B: Polym. Phys, . (2004) 4326-4336.
[16] M. Sandru, T.-J. Kim, M.-B. Hägg, High molecular fixed-site-carrier PVAm membrane for CO_2 capture, Desalination, 240 (2009) 298-300.
[17] J. Kim, Q. Fu, K. Xie, J.M.P. Scofield, S.E. Kentish, G.G. Qiao, CO_2 separation using surface-functionalized SiO2 nanoparticles incorporated ultra-thin film composite mixed matrix membranes for post-combustion carbon capture, J. Membr. Sci., 515 (2016) 54-62.
[18] T. Markel, Membrane process to sequester CO_2 from power plant flue gas, The U.S. Department of Energy, NETL, July 2009.
[19] P.M. Budd, N.B. McKeown, D. Fritsch, Polymers of Intrinsic Microporosity (PIMs): High Free Volume Polymers for Membrane Applications, Macromol. Symp., 245-246 (2006) 403-405.
[20] S. Kim, Y.M. Lee, Rigid and microporous polymers for gas separation membranes, Progr. Polym. Sci., 43 (2015) 1-32.
[21] T. Masuda, E. Isobe, T. Higashimura, K. Takada, Poly[1-(trimethylsilyl)-1-propyne]: a new high polymer synthesized with transition-metal catalysts and characterized by extremely high gas permeability, J. Amer. Chem. Soc., 105 (1983) 7473-7474.
[22] N. Du, H.B. Park, G.P. Robertson, M.M. Dal-Cin, T. Visser, L. Scoles, M.D. Guiver, Polymer nanosieve membranes for CO_2-capture applications, Nat. Mater., 10 (2011) 372-375.
[23] A.F. Bushell, P.M. Budd, M.P. Attfield, J.T.A. Jones, T. Hasell, A.I. Cooper, P. Bernardo, F. Bazzarelli, G. Clarizia, J.C. Jansen, Nanoporous Organic Polymer/Cage Composite Membranes, Angew. Chem. Int. Edn., 52 (2013) 1253-1256.
[24] C.H. Lau, K. Konstas, C.M. Doherty, S. Kanehashi, B. Ozcelik, S.E. Kentish, A.J. Hill, M.R. Hill, Tailoring Physical Aging in Super Glassy Polymers with Functionalized Porous Aromatic Frameworks for CO_2 Capture, Chem. Mater., 27 (2015) 4756-4762.

[25] C.H. Lau, P.T. Nguyen, M.R. Hill, A.W. Thornton, K. Konstas, C.M. Doherty, R.J. Mulder, L. Bourgeois, A.C.Y. Liu, D.J. Sprouster, J.P. Sullivan, T.J. Bastow, A.J. Hill, D.L. Gin, R.D. Noble, Ending Aging in Super Glassy Polymer Membranes, Angew. Chem. Int. Edn., 53 (2014) 5322-5326.
[26] C.H. Lau, K. Konstas, A.W. Thornton, A.C.Y. Liu, S. Mudie, D.F. Kennedy, S.C. Howard, A.J. Hill, M.R. Hill, Gas-Separation Membranes Loaded with Porous Aromatic Frameworks that Improve with Age, Angew. Chem. Int. Edn., 54 (2015) 2669-2673.
[27] B. Li, X. Huang, L. Liang, B. Tan, Synthesis of uniform microporous polymer nanoparticles and their applications for hydrogen storage, J. Mater. Chem., 20 (2010) 7444-7450.
[28] J.-S.M. Lee, M.E. Briggs, T. Hasell, A.I. Cooper, Hyperporous Carbons from Hypercrosslinked Polymers, Adv. Mater., 28 (2016) 9804-9810.
[29] J. Albo, H. Hagiwara, H. Yanagishita, K. Ito, T. Tsuru, Structural Characterization of Thin-Film Polyamide Reverse Osmosis Membranes, Ind. Eng. Chem. Res., 53 (2014) 1442-1451.
[30] J. Albo, J.H. Wang, T. Tsuru, Application of interfacially polymerized polyamide composite membranes to isopropanol dehydration: Effect of membrane pre-treatment and temperature, J. Membr. Sci., 453 (2014) 384-393.
[31] J. Albo, J.H. Wang, T. Tsuru, Gas transport properties of interfacially polymerized polyamide composite membranes under different pre-treatments and temperatures, J. Membr. Sci., 449 (2014) 109-118.
[32] A. Bhaskar, R. Banerjee, U. Kharul, ZIF-8@PBI-Bul composite membranes: elegant effects of PBI structural variations on gas permeation performance, J. Mater. Chem. A, 2 (2014) 12962-12967.
[33] K.S.W. Sing, D.H. Everett, R.A.W. Haul, L. Moscou, R.A. Pierotti, J. Rouquerol, T. Siemieniewska, Reporting Physisorption Data for Gas Solid Systems with Special Reference to the Determination of Surface-Area and Porosity (Recommendations 1984), Pure Appl. Chem., 57 (1985) 603-619.
[34] I. Luzinov, D. Julthongpiput, H. Malz, J. Pionteck, V.V. Tsukruk, Polystyrene layers grafted to epoxy-modified silicon surfaces, Macromolecules, 33 (2000) 1043-1048.
[35] P.H. Chen, D.D.L. Chung, Dynamic mechanical behavior of flexible graphite made from exfoliated graphite, Carbon, 50 (2012) 283-289.
[36] R.T. Woodward, L.A. Stevens, R. Dawson, M. Vijayaraghavan, T. Hasell, I.P. Silverwood, A.V. Ewing, T. Ratvijitvech, J.D. Exley, S.Y. Chong, F. Blanc, D.J. Adams, S.G. Kazarian, C.E. Snape, T.C. Drage, A.I. Cooper, Swellable, Water- and Acid-Tolerant Polymer Sponges for Chemoselective Carbon Dioxide Capture, J. Amer. Chem. Soc., 136 (2014) 9028-9035.
[37] C.D. Wood, B. Tan, A. Trewin, H.J. Niu, D. Bradshaw, M.J. Rosseinsky, Y.Z. Khimyak, N.L. Campbell, R. Kirk, E. Stockel, A.I. Cooper, Hydrogen storage in microporous hypercrosslinked organic polymer networks, Chem. Mater., 19 (2007) 2034-2048.
[38] G. Horvath, K. Kawazoe, Method for the Calculation of Effective Pore-Size Distribution in Molecular-Sieve Carbon, J. Chem. Eng. Jpn., 16 (1983) 470-475.
[39] S.Y. Lee, S.J. Park, Carbon dioxide adsorption performance of ultramicroporous carbon derived from poly(vinylidene fluoride), J. Anal. Appl. Pyrol., 106 (2014) 147-151.
[40] D.E. Sanders, Z.P. Smith, R.L. Guo, L.M. Robeson, J.E. McGrath, D.R. Paul, B.D. Freeman, Energy-efficient polymeric gas separation membranes for a sustainable future: A review, Polymer, 54 (2013) 4729-4761.
[41] J. Ahn, W.J. Chung, I. Pinnau, J.S. Song, N.Y. Du, G.P. Robertson, M.D. Guiver, Gas transport behavior of mixed-matrix membranes composed of silica nanoparticles in a polymer of intrinsic microporosity (PIM-1), J. Membr. Sci., 346 (2010) 280-287.
[42] J.C. Maxwell, A treatise on electricity and magnetism, Oxford University Press, Oxford, 1873.
[43] M.R. Khdhayyer, E. Esposito, A. Fuoco, M. Monteleone, L. Giorno, J.C. Jansen, M.P. Attfield, P.M. Budd, Mixed matrix membranes based on UiO-66 MOFs in the polymer of intrinsic microporosity PIM-1, Sep. Purif. Technol., 173 (2017) 304-313.
[44] P. Bernardo, E. Bazzarelli, F. Tasselli, G. Clarizia, C.R. Mason, L. Maynard-Atem, P.M. Budd, M. Lanc, K. Pilnacek, O. Vopicka, K. Friess, D. Fritsch, Y.P. Yampolskii, V. Shantarovich, J.C. Jansen, Effect of physical aging on the gas transport and sorption in PIM-1 membranes, Polymer, 113 (2017) 283-294.
[45] K.D. Dorkenoo, P.H. Pfromm, Accelerated physical aging of thin poly[1-(trimethylsilyl)-1-propyne] films, Macromolecules, 33 (2000) 3747-3751.

[46] R.R. Tiwari, Z.P. Smith, H.Q. Lin, B.D. Freeman, D.R. Paul, Gas permeation in thin films of "high free-volume" glassy perfluoropolymers: Part I. Physical aging, Polymer, 55 (2014) 5788-5800.
[47] T. Koschine, K. Ratzke, F. Faupel, M.M. Khan, T. Emmler, V. Filiz, V. Abetz, L. Ravelli, W. Egger, Correlation of Gas Permeation and Free Volume in New and used High Free Volume Thin Film Composite Membranes, J. Polym. Sci. Pol. Phys., 53 (2015) 213-217.
[48] R.R. Tiwari, J.Y. Jin, B.D. Freeman, D.R. Paul, Physical aging, CO2 sorption and plasticization in thin films of polymer with intrinsic microporosity (PIM-1), J. Membr. Sci., 537 (2017) 362-371.
[49] S. Harms, K. Rätzke, F. Faupel, N. Chaukura, P.M. Budd, W. Egger, L. Ravelli, Aging and Free Volume in a Polymer of Intrinsic Microporosity (PIM-1), J. Adhesion, 88 (2012) 608-619.
[50] M. Sadeghi, M.A. Semsarzadeh, H. Moadel, Enhancement of the gas separation properties of polybenzimidazole (PBI) membrane by incorporation of silica nano particles, J. Membr. Sci., 331 (2009) 21-30.
[51] I. Rose, C.G. Bezzu, M. Carta, B. Comesana-Gandara, E. Lasseuguette, M.C. Ferrari, P. Bernardo, G. Clarizia, A. Fuoco, J.C. Jansen, K.E. Hart, T.P. Liyana-Arachchi, C.M. Colina, N.B. McKeown, Polymer ultrapermeability from the inefficient packing of 2D chains, Nat. Mater., 16 (2017) 932-+.
[52] Y. Liu, J. Liu, Y.S. Lin, M. Chang, Effects of Water Vapor and Trace Gas Impurities in Flue Gas on CO_2/N_2 Separation Using ZIF-68, J. Phys. Chem. C, 118 (2014) 6744-6751.
[53] S. Kanehashi, G.Q. Chen, L. Ciddor, A. Chaffee, S.E. Kentish, The impact of water vapor on CO_2 separation performance of mixed matrix membranes, J. Membr. Sci., 492 (2015) 471-477.
[54] A. Car, C. Stropnik, W. Yave, K.-V. Peinemann, Pebax®/polyethylene glycol blend thin film composite membranes for CO_2 separation: Performance with mixed gases, Sep. Purif. Technol., 62 (2008) 110-117.
[55] Q. Fu, J. Kim, P.A. Gurr, J.M.P. Scofield, S.E. Kentish, G.G. Qiao, A novel cross-linked nano-coating for carbon dioxide capture, Energy Environ. Sci., 9 (2016) 434-440.
[56] C.M. Spadaccini, E.V. Mukerjee, S.A. Letts, A. Maiti, K.C. O'Brien, Ultrathin polymer membranes for high throughput CO_2 capture, Energy Procedia, 4 (2011) 731-736.
[57] A. Halim, Q. Fu, Q. Yong, P.A. Gurr, S.E. Kentish, G.G. Qiao, Soft polymeric nanoparticle additives for next generation gas separation membranes, J. Mater. Chem. A, 2 (2014) 4999-5009.
[58] J.X. Zhou, M.M. Tran, A.T. Haldeman, J.Y. Jin, E.H. Wagener, S.M. Husson, Perfluorocyclobutyl polymer thin-film composite membranes for CO_2 separations, J. Membr. Sci., 450 (2014) 478-486.
[59] D.S. Bakhtin, L.A. Kulikov, S.A. Legkov, V.S. Khotimskiy, I.S. Levin, I.L. Borisov, A.L. Maksimov, V.V. Volkov, E.A. Karakhanov, A.V. Volkov, Aging of thin-film composite membranes based on PTMSP loaded with porous aromatic frameworks, J. Membr. Sci., 554 (2018) 211-220.
[60] M.M. Khan, V. Filiz, G. Bengtson, S. Shishatskiy, M. Rahman, V. Abetz, Functionalized carbon nanotubes mixed matrix membranes of polymers of intrinsic microporosity for gas separation, Nanoscale Res. Lett., 7 (2012) 1-12.
[61] S.D. Bazhenov, I.L. Borisov, D.S. Bakhtin, A.N. Rybakova, V.S. Khotimskiy, S.P. Molchanov, V.V. Volkov, High-permeance crosslinked PTMSP thin-film composite membranes as supports for CO_2 selective layer formation, Green Energy Environ., 1 (2016) 235-245.

SUPPORTING INFORMATION

Ultrahigh-permeance PIM-1 based thin film nanocomposite membranes on PAN supports for CO_2 separation

Rupesh S. Bhavsar,[a1] Tamoghna Mitra,[b1]
Dave J. Adams,[c*] Andrew I. Cooper,[b*] Peter M. Budd[a*]

[a]School of Chemistry, University of Manchester, Manchester M13 9PL, UK
[b]Department of Chemistry, University of Liverpool, Crown Street, Liverpool, Merseyside L69 7ZD, UK
[c]School of Chemistry, College of Science and Engineering, University of Glasgow, Glasgow, G12 8QQ, UK
[1]These authors contributed equally to this work
[*]Corresponding author

E-mail addresses: Peter.Budd@manchester.ac.uk (Peter. M. Budd)
aicooper@liverpool.ac.uk (Andrew I. Cooper)
dave.adams@glasgow.ac.uk (Dave J. Adams)

CONTENTS

1. Synthesis and characterization of PIM-1

To a dry 500 mL round bottom flask equipped with a Dean−Stark trap and mechanical stirrer, 5,5′,6,6′-tetrahydroxy-3,3,3′,3′-tetramethyl-1,1′-spirobisindane (17.288 g, 0.05 mol) and dicyanotetrafluorobenzene (10.005 g, 0.05 mol), anhydrous K_2CO_3 (20.73 g, 0.15 mol), dimethylacetamide (100 mL) and toluene (50 mL) were added under an inert atmosphere of nitrogen. The temperature was raised to 160 °C over a 15 min time period, and maintained at that temperature under reflux for 45 min. At the end of the reaction, when stirring was stopped, the highly viscous solution was immediately poured into methanol (500 mL). Following this, it was dissolved in chloroform (500 mL) and reprecipitated from methanol (2 L). The product was refluxed for 15 h in deionized water, washed with acetone and then dried at 110 °C for 2 days. Average molar masses were measured by a Viscotek VE2001 GPC system with Viscotek 3580 refractive index detector, using THF as the eluent at a flow rate of 1 mL min^{-1}. The data were analysed using OmniSEC software. ^1H nuclear magnetic resonance (NMR) spectra of the parent polymers were recorded using a Bruker Avance II 500 MHz instrument. Polymer solutions for NMR were prepared in $CDCl_3$. Elemental analysis was carried out by the School of Chemistry Microanalysis Service, University of Manchester, using a Thermo Scientific Flash 2000 organic elemental analyzer (CHNS analyser).

GPC (in THF): M_w = 120000 g mol^{-1}, M_w/M_n = 3.1. ^1H NMR (500 MHz, $CDCl_3$, δ, ppm): 6.75 (2H, s), 6.35 (2H, s), 2.26−2.09 (4H, dd), 1.40−1.10 (broad, 12H). Anal. Calc. for $C_{29}H_{20}N_2O_4$ (wt %): C, 75.64; H, 4.37; N, 6.08. Found: C, 74.64; H, 4.37; N, 6.03.

2. Synthesis of HCP nanoparticles

2.1 Synthesis of polyvinyl benzyl chloride precursor particles

0.45 g (5.6 wt% based on vinylbenzyl chloride) sodium dodecyl sulphate was dissolved in distilled water (80 mL) and added to a 500 mL three-necked round bottom flask. Then the inhibitor freed co-monomer mixture (vinylbenzyl chloride, 8 g, *p*-divinylbenzene, 2 wt%, 0.20 g) was added and pre-emulsified using a mechanical stirrer at 400 rpm under N_2 for 30 min. An aqueous solution of potassium persulphate (1 wt% based on vinylbenzyl chloride, 0.082 g in 2 mL) was added to the above mixture at 80 °C, and the emulsion polymerization was carried out using a mechanical stirrer at 400 rpm under N_2 for 5 h. The emulsions were broken by drop-wise addition into stirring methanol (200 mL), and then the white nanoparticles were isolated by centrifugation and washed three times with distilled water, methanol, and diethyl ether, followed by drying for 24 h at 60 °C.

2.2 Synthesis of HCP particles

The precursor nanoparticles of polyvinylbenzyl chloride (2.5 g) were swollen in 40 mL dry dichloroethane (DCE) under inert atmosphere for 3 h. A suspension of $FeCl_3$ (2.61 g) in dichloroethane (40 mL) was added to the nanoparticle suspension, which was then heated at 80 °C for 18 h. The resulting hypercrosslinked products were filtered and washed three times with distilled water, methanol, and diethyl ether, followed by soxhlet extraction in methanol for 24 h, finally drying for 24 h at 60 ˚C.

3. Thermal gravimetric analysis

Thermal gravimetric analysis of PIM-1, HCP and C-HCP was carried out using a TGA Q5000 IR Thermogravimetric Analyzer, with 10 ºC/min heating ramp under nitrogen flow. Results are shown in Figure S1.

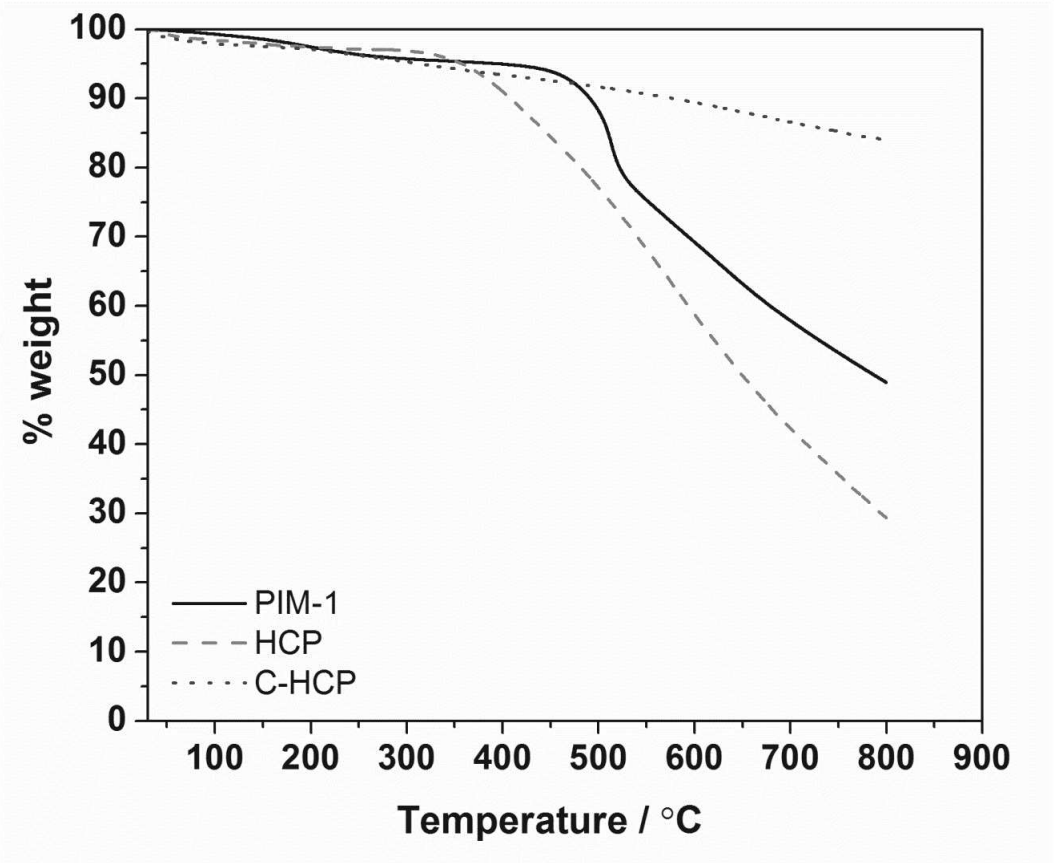

Fig. S1. Thermal gravimetric analysis of PIM-1, HCP and C-HCP.

4. Preparation of self-standing MMMs

MMMs of PIM-1 with C-HCP in three different proportions (4.8 wt%, 9.1 wt% and 16. 7 wt% C-HCP) were prepared by casting from solution in $CHCl_3$ as described previously for PIM-1/HCP MMMs [1]. For preparation of MMMs containing 16.7 wt% C-HCP, a suspension of filler (0.06 g) in 5 mL $CHCl_3$ was stirred for 12 h at ambient temperature, followed by sonication for 30 min in an ultrasonic bath at ambient temperature. A $CHCl_3$ solution of PIM-1 (0.3 g in 5 mL $CHCl_3$) was added to the suspension and the mixture stirred for 20 h. The resulting solution was sonicated for 20 min in an ultrasonic bath at ambient temperature before being poured into a 9 cm glass petri dish. The membrane was allowed to form by slow solvent evaporation over 24-36 hours in a N_2 environment. The membranes were then kept in a desiccator for 24 h under vacuum before analysis.

Weight percentage of filler in all MMMs prepared was calculated as

$$\text{Wt\% of filler in MMM} = \frac{100 \times \text{wt. of filler}}{\text{wt. of filler} + \text{wt. of PIM - 1}}$$

Photographs of ethanol-treated MMMs are shown in Figure S2. PIM-1/C-HCP membranes are black, due to the presence of the filler phase.

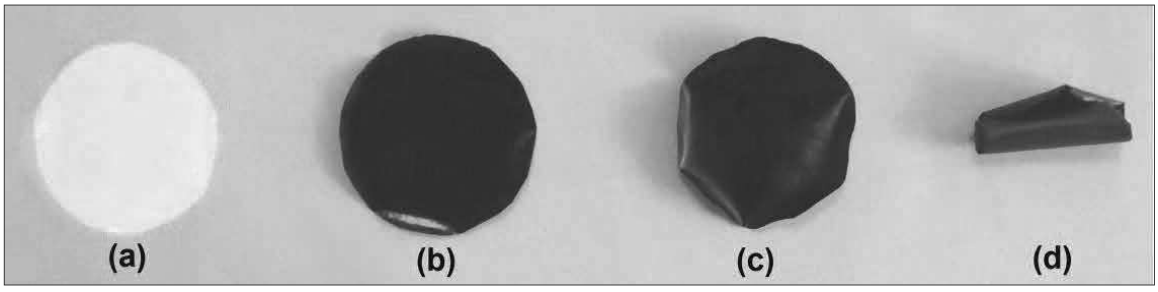

Fig. S2. Photographs of ethanol-treated PIM-1/C-HCP MMMs. (a) PIM-1, (b) PIM-1/C-HCP 4.8 wt%, (c) PIM-1/C-HCP 9.1 wt%, (d) PIM-1/C-HCP 16.7 wt%.

5. Scanning Electron Microscopy

The filler and membrane morphologies were studied by scanning electron microscopy (SEM) using a Hitachi S-4800 Field-Emission Scanning Electron Microscope with Energy Dispersive X-Ray (EDX) detector and cold cathode electron source. Membrane cross sections were prepared via freeze fracturing using liquid nitrogen. The samples were then coated with gold via sputtering using an Emitech coater.

The HCP and C-HCP nanoparticles showed spherical morphology as seen in Figure S3.

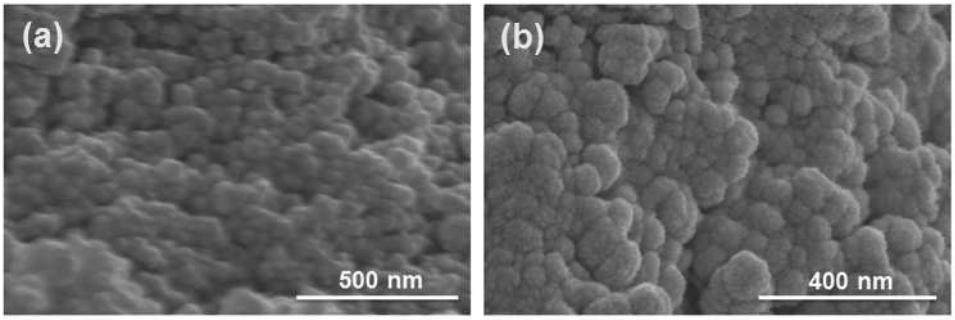

Fig. S3. SEM images of (a) HCP and (b) C-HCP.

6. Membrane characterization

The PAN ultrafiltration membrane used as a support showed a narrow pore size distribution with a pore size ~ 31 nm, as shown by the SEM image and porometer data in Figure S4.

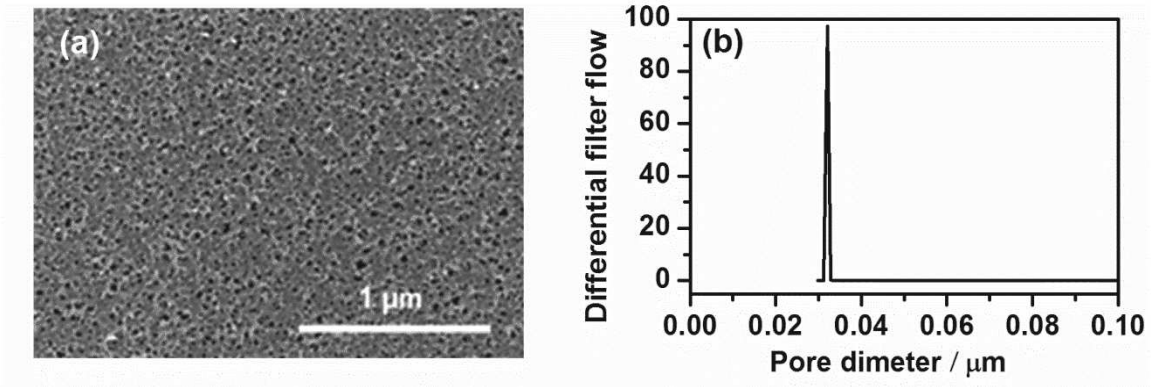

Fig. S4. Sepro PA350 PAN support: (a) SEM image courtesy of Ingo Pinnau, Functional Polymer Membranes Group, King Abdullah University of Science and Technology; (b) pore size distribution determined by Porolux^{TM} 1000 Porometer.

SEM of the PIM-1/C-HCP and PIM-1/HCP TFN membranes showed a reasonably homogeneous distribution of the filler (Figures S5, S6). At higher filler loading, TFN membranes had irregular surface layers of varying thickness.

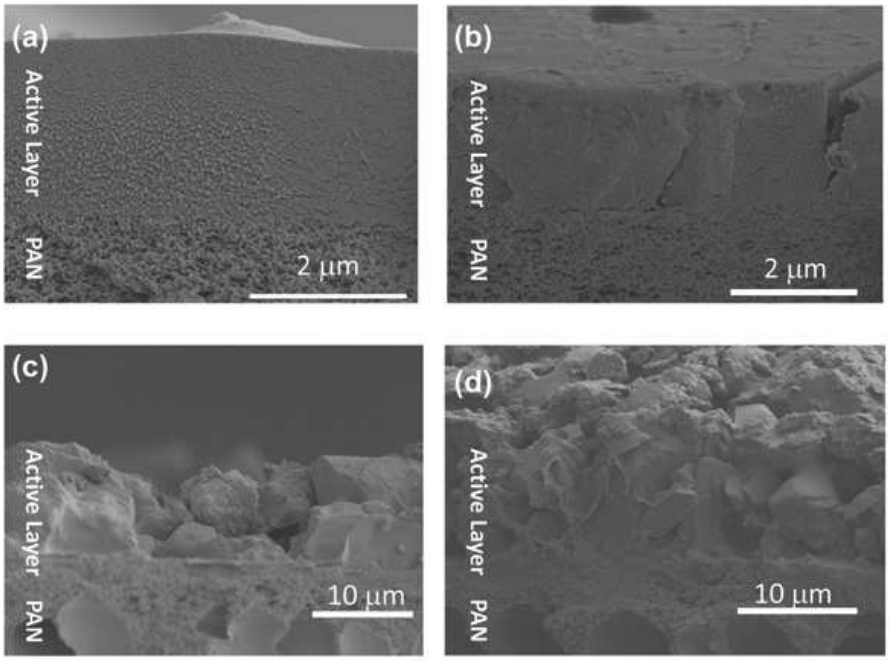

Fig. S5. SEM of PIM-1/C-HCP thin film nanocomposite membranes: (a) PIM-1/C-HCP 10 wt%, (b) PIM-1/C-HCP 20 wt%, (c) PIM-1/C-HCP 40 wt%, (d) PIM-1/C-HCP 60 wt%

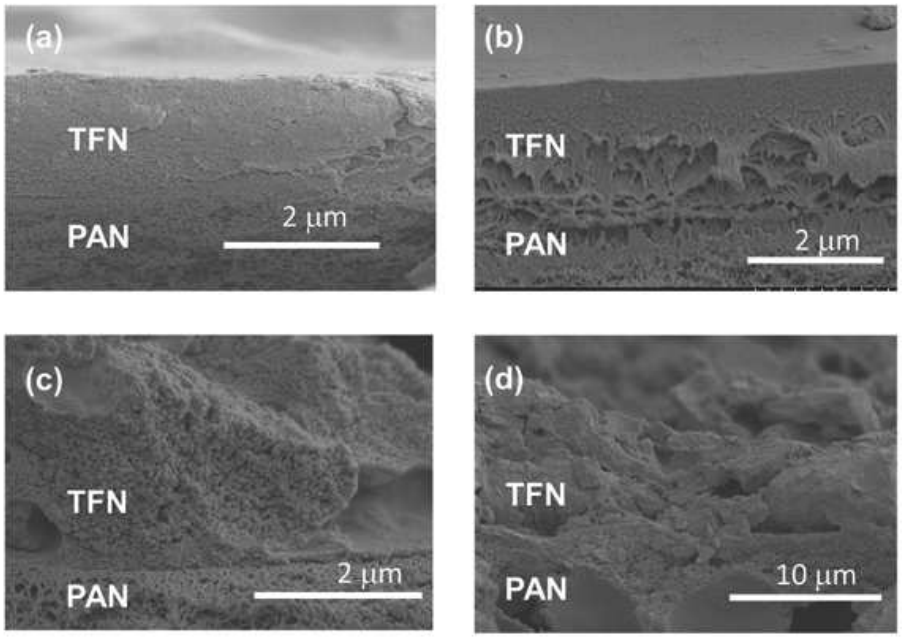

Fig. S6. SEM of PIM-1/HCP thin film nanocomposite membranes: (a) PIM-1/HCP 10 wt%, (b) PIM-1/HCP 20 wt%, (c) PIM-1/HCP 40 wt%, (d) PIM-1/HCP 60 wt%.

7. Gas permeation

The variable volume method was used for the determination of gas permeability. A schematic of the permeation equipment and a photograph of the permeation cell are shown in Figure S7. One end of the feed side of the cell was connected through valve V_1 to the feed gas cylinder outlet and a pressure gauge (1-10 atm range). The valve V_2 was vent and used to control the feed pressure. On the permeate side of the cell, a bubble flowmeter was connected. The permeability measurements using pure gases (CO_2 and N_2) were carried out as described in the manuscript. The data obtained are given in Tables S1-S4.

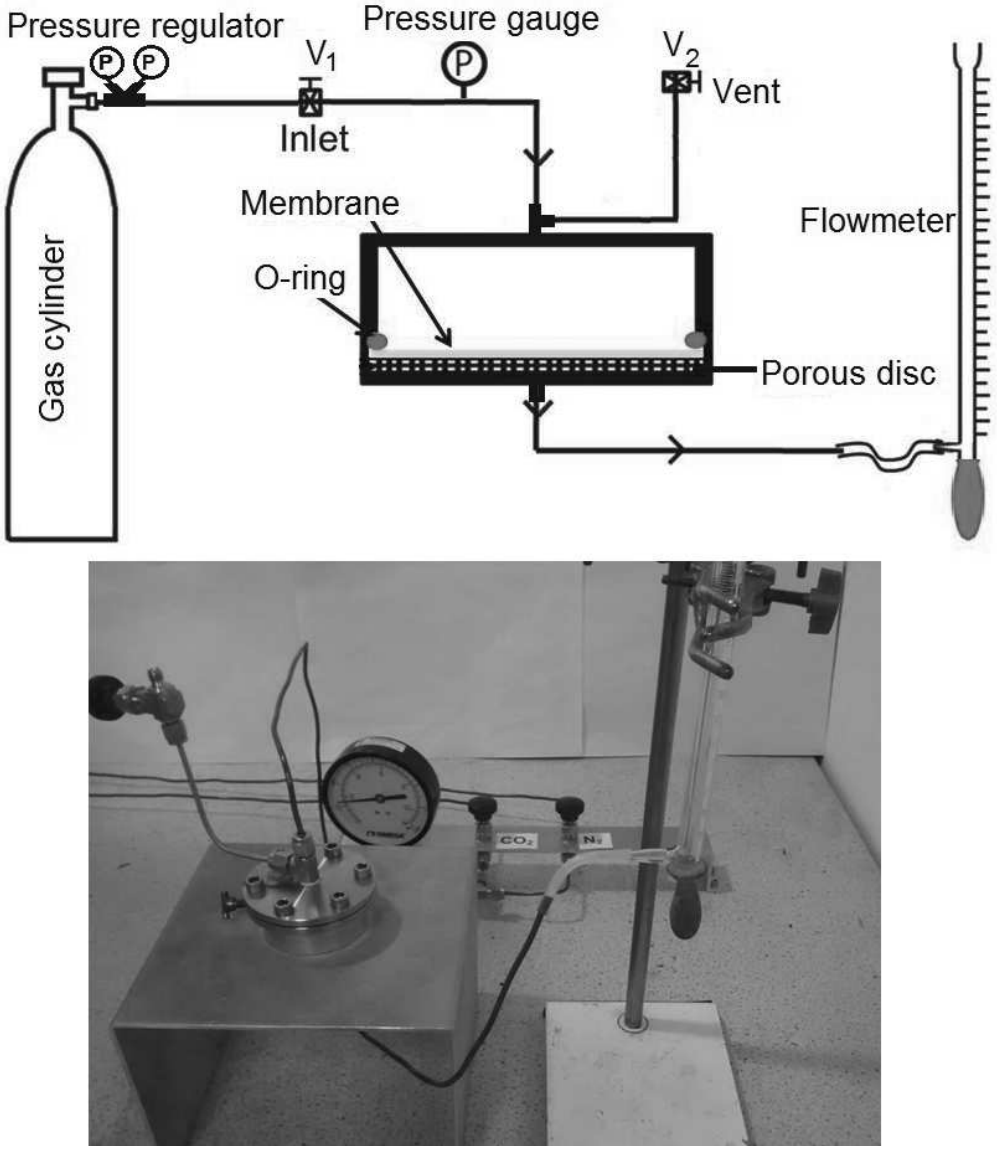

Fig. S7. Schematic and photograph of gas permeation equipment.

Table S1. Single gas permeation data for PIM-1/C-HCP TFN membranes. *K* is permeance and α is the selectivity determined as a ratio of fluxes. Also given is the average selective layer thickness as measured by SEM (± indicates one standard deviation).

Filler concentration (wt %)	**Selective layer thickness (μm)**	**Age (Days)**	***K*(CO_2) (GPU*)**	***K*(N_2) (GPU*)**	**α(CO_2/N_2)**
0 (PIM-1)	2.08	1	3331	234	14.2
		7	1441	77	18.6
		30	826	35	23.6
		50	562	24	23.3
		90	388	16	24.5
10	2.02 ± 0.28	1	5341	439	12.2
		7	2529	161	15.7
		30	1291	80	16.2
		50	899	50	18.0
		90	553	31	17.7
20	1.62 ± 0.09	1	6316	633	10.0
		7	3034	217	14.0
		30	1497	104	14.4
		50	1436	97	14.8
		90	1266	87	14.5
40	6.94 ± 1.80	1	15645	1695	9.2
		7	7418	503	14.8
		30	4015	277	14.5
		50	3271	233	14.0
		90	2800	207	13.5
60	8.05 ± 1.99	1	27530	4197	6.6
		7	15352	1652	9.3
		30	11648	918	12.7
		50	10310	847	12.2
		90	9379	834	11.3

*1 GPU = 10^{-6} cm^3 [STP] cm cm^{-2} s^{-1} $cmHg^{-1}$

Table S2. Single gas permeation data for PIM-1/HCP TFN membranes. *K* is permeance and α is the selectivity determined as a ratio of fluxes. Also given is the average selective layer thickness as measured by SEM (± indicates one standard deviation).

Filler concentration (wt %)	**Selective layer thickness (µm)**	**Age (Days)**	***K*(CO_2) (GPU*)**	***K*(N_2) (GPU*)**	**α(CO_2/N_2)**
0 (PIM-1)	2.08	1	3331	234	14.2
		7	1441	77	18.6
		30	826	35	23.6
		50	562	24	23.3
		90	388	16	24.5
10	1.63 ± 0.1	1	4069	352	11.6
		7	2047	133	15.4
		30	277	14	20.5
		90	207	10	20.6
20	1.76 ± 0.2	1	5935	541	11.0
		7	3131	221	14.2
		30	301	16	18.4
		90	291	15	19.7
40	1.38 ± 0.69	1	10028	1055	9.5
		7	5022	424	11.8
		30	637	63	10.1
		90	556	50	11.2
60	6.32 ± 1.18	1	21627	4199	5.2
		7	9595	1431	6.7
		30	7515	920	8.2
		90	6839	869	7.9

*1 GPU = 10^{-6} cm^3 [STP] cm cm^{-2} s^{-1} $cmHg^{-1}$

Table S3. Single gas permeation data for as cast PIM-1/C-HCP self-standing MMMs. *P* is permeability coefficient.

Filler concentration (wt %)	Thickness (µm)	$P(CO_2)$ (barrer*)	$P(N_2)$ (barrer*)	$\alpha(CO_2/N_2)$
0 (PIM-1)	41 ± 3.5	2437	109	22.4
4.8	54.7 ± 2	7918	534	14.8
9.1	65.8 ± 4.5	9928	681	14.6
16.7	89.6 ± 5.6	14026	923	15.2

*1 barrer = 10^{-10} cm^3 [STP] cm cm^{-2} s^{-1} $cmHg^{-1}$

Table S4. Single gas permeation data for ethanol treated PIM-1/C-HCP self-standing MMMs. *P* is permeability coefficient.

Filler concentration (wt %)	Thickness (µm)	Age (Days)	$P(CO_2)$ (barrer*)	$P(N_2)$ (barrer*)	$\alpha(CO_2/N_2)$
0 (PIM-1)	54 ± 1.5	1	7532	502	15.0
		30	5342	252	21.2
		90	3016	124	24.3
		150	2535	103	24.7
		200	1985	84	23.6
4.8	58 ± 0.7	1	10489	766	13.7
		90	7495	452	16.6
		150	7322	439	16.7
		200	5303	314	16.9
9.1	75 ± 4.4	1	13355	971	13.8
		90	10036	631	15.9
		150	8594	532	16.2
		200	7088	399	17.8

*1 barrer = 10^{-10} cm^3 [STP] cm cm^{-2} s^{-1} $cmHg^{-1}$

8. Reference

[1] T. Mitra, R.S. Bhavsar, D.J. Adams, P.M. Budd, A.I. Cooper, PIM-1 mixed matrix membranes for gas separations using cost-effective hypercrosslinked nanoparticle fillers, *Chem. Commun*., 52 (2016) 5581-5584.